



Qualification Tests of COTS Aeroguard® Thermal Protection Panels used for the Hexafly-Int Hypersonic Glider

Sébastien Paris¹, Jean-Baptiste Gouriet², Jimmy Freitas Monteiro³, Johan Steelant⁴

Abstract

This paper deals with the qualification tests of the COTS Aeroguard® thermal protection panels used as internal Thermal Control System (TCS) inside the Hexafly-Int glider and as external Thermal Protection System (TPS) of its service module dedicated to the insertion into the atmosphere. Three different set of tests were performed: (i) Oven tests so as to qualify the thermal behaviour of the TCS especially when submitted to depressurization inside the vehicle which is supposed to reduce by an order of the magnitude the thermal conductivity of the panels (ii) Centrifuge tests so as to assess the mechanical strength of different types of fixations between the airframe and the TCS during the boosted ascent phase of the flight (iii) Wind tunnel tests so as to assess the strength of ESM external thermal protection panels. The main results are: (i) Insulation properties of the internal TCS is much less as expected and will lead to a redesign of the TCS (ii) The fixations based on lateral traps made with Velcro are far from the most resistant with respect to g-loads (iii) External panels of the ESM are able to withstand the aerodynamic load.

Keywords: *Thermal Protection Panels, Oven tests, Centrifuge tests, Wind tunnel tests*

Nomenclature (Tahoma 11 pt, bold)

EFTV	Experimental Flight Test Vehicle
ESM	Experimental Service Module
TCS	Thermal Control System
TPS	Thermal Protection System

¹ Von Karman Institute, Chaussée de Waterloo, 72 – 1640 Rhode Saint Genèse, Belgium, paris@vki.ac.be

² Von Karman Institute, Chaussée de Waterloo, 72 – 1640 Rhode Saint Genèse, Belgium, gouriet@vki.ac.be

³ Von Karman Institute, Chaussée de Waterloo, 72 – 1640 Rhode Saint Genèse, Belgium, jimmy.freitas.monteiro@vki.ac.be

⁴ ESA-ESTEC, Aerothermodynamics and Propulsion Analysis Section TEC-MPA, P.O. Box 299, Noordwijk, Netherlands, Johan.Steelant@esa.int

1. Introduction

The Hexafly-Int vehicle is a 3 m long hypersonic glider which will be launched on top of a single stage sounding rocket up to an altitude of nearly 90 km. After the apogee, the Experimental Flight Test Vehicle (EFTV) will perform a first part of the descent trajectory aided by an Experimental Service Module (ESM), then after the separation it will perform a pull-out manoeuvre, to finally starting a gliding phase at Mach 8 at an altitude of nearly 30 000 m during few hundreds of seconds. The glider aeroshape design makes maximum use of databases, expertise, technologies and materials elaborated in previously European community co-funded projects LAPCAT I & II [1][2], ATLLAS I & II [3][4] and HEXAFly [5].

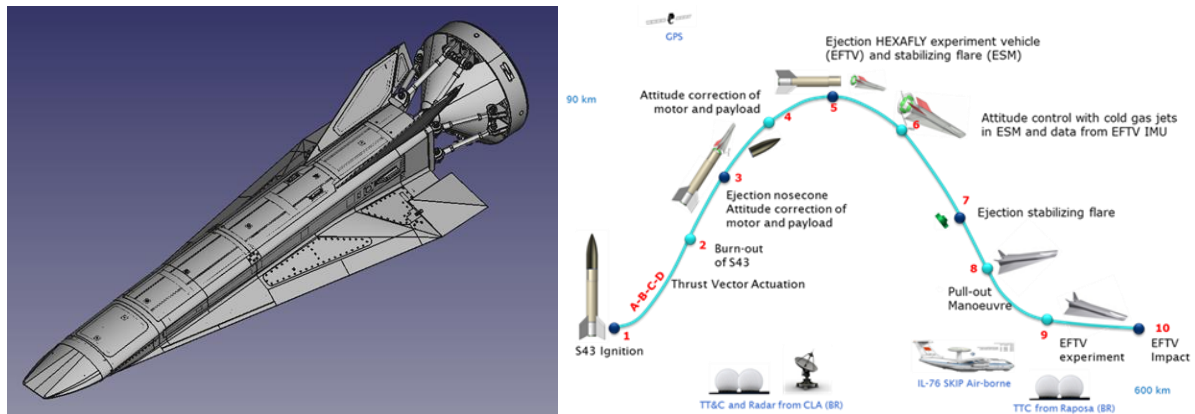


Fig. 1: Hexafly-Int EFTV+ESM and profile mission

Equipment inside the EFTV is supposed to be protected from radiation of the airframe thanks to two 9 mm thick thermal protection layers put on the internal faces of the fuselage [6]. Those layers are made of Aeroguard® panels manufactured by Belgium PROMAT society. The thicknesses of the layers were calculated by supposing that the air pressure inside the panels is instantaneously equal to the air pressure inside the EFTV, which induces that the thermal conductivity of the panel is an order of magnitude lower than at sea level pressure on the basis of data provided by PROMAT. The first part of this study is dedicated to the qualification of the thermal properties. Aeroguard® panels are also supposed to be used as external Thermal Protection System of the mechanical links between the main body of the ESM and the four struts insuring the connection between the ESM and the EFTV. As the material is directly exposed to the flow, tests in representative environment will be conducted. The second part of the project intend to verify the capability of the material to support this aerodynamic load. During the flight, the insulating material will be subject to high acceleration. The TCS, covering the internal wall of the vehicle must be properly fixed in order to sustain this load. Finally, static load tests will performed at the Large Diameter Centrifuge (LCD) at ESA/ESTEC to qualify the fixations of the AEROGUARD insulation panels on the structure of the vehicle.

2. Thermal qualification of the internal TCS of the EFTV

The objective of this task is to characterise experimentally the heat transfer through a representative multilayer assembly, i.e. Titanium shell combined with two layers of insulation panels on its backside, at representative pressure evolution experienced during the flight, i.e. from ambient pressure down to near vacuum. This paper details the laboratory tests and related thermal database as well as the restitution of these tests with a nodal model in order to derive the thermal properties of the assembly.

2.1. experimental apparatus

Fig. 2 (left) shows the experimental apparatus assembled for the thermal characterisation of the multilayer assembly (i.e. one layer of Titanium Ti-6Al-4V and two layers of Aeroguard 160 SD). The experimental apparatus is composed of a closed (leak tight) thermal cell in Titanium, which is connected to a vacuum pump and a pressure sensor. Its front face exposed to the radiative heat flux is insulated on its backside with two layers of Aeroguard 160 SD. The cell is partially inserted inside a high-temperature furnace as illustrated in Fig. 2 (right). The multi-layer assembly is instrumented with several thermocouples for its thermal characterisation. Additional thermocouples are also used to monitor or control the thermal boundary conditions (i.e. temperature regulation of the furnace...). The vacuum line connecting the cell to the vacuum pump is equipped with a regulating valve and a solenoid valve to control the depressurisation rate imposed during the tests. Finally, a PC-based measurement and control system completes the experimental apparatus. More details on the experimental apparatus are provided in [7].

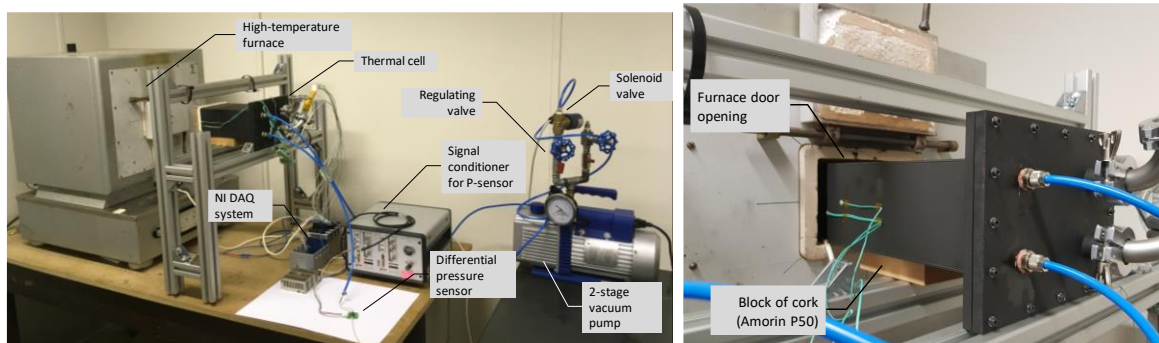


Fig. 2: Experimental apparatus - thermal cell outside the furnace (left) and inside the furnace (right)

Fig. 3 show a cut view of the thermal cell respectively in its calibration and testing configuration. This cell is made of Titanium Ti-6Al-4V panels (3mm thick) assembled and laser welded together. The cell is closed in its back with a rectangular flange. A thick partition plate is inserted into the cell in order to limit its deformation when the depressurisation is applied. All the surfaces of the test cell including the partition plate and the flange are covered with a black paint with an emissivity ϵ of 0.9.

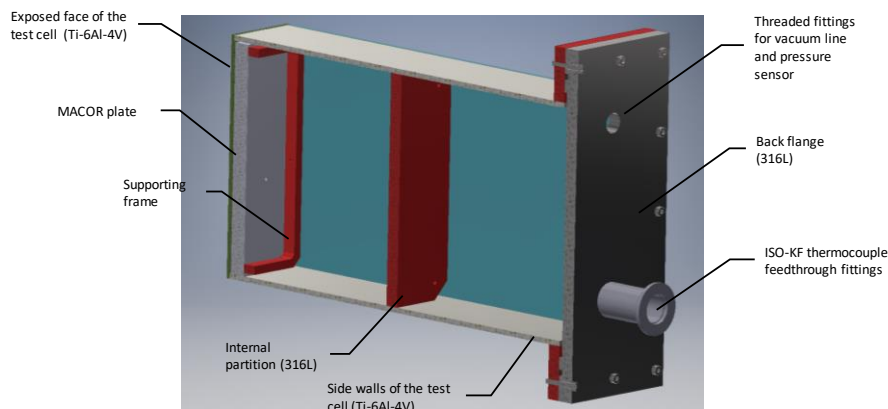


Fig. 3: Test cell in calibration configuration

The cell has been used first for the calibration tests. A 10mm thick plate made of a reference material and instrumented with thermocouples is placed on the backside of the front face (Fig. 3). This plate is kept in place with a supporting frame fixed to the sidewalls with four compression screws. The reference material is a glass ceramic material MACOR. This zero-porosity and non-outgassing material is particularly interesting for calibration since it has a moderate thermal conductivity around $1.5\text{W/m}^2\cdot\text{K}$

which allows measuring with a reasonable accuracy the temperature jump across this material and therefore assessing the heat flux with the Fourier's law.

For the thermal tests, the calibration plate is replaced by two layers of Aeroguard 160 SD (SD = Standard Duty rated at 500°C, thickness of a single layer = 9mm). These layers are placed against the wall without applying any particular compression force on them. They are kept in place with the supporting frame as for the calibration plate. Finally, the two layers are instrumented with a series of thermocouples to measure the temperature distribution across them.

2.2. Calibration

The calibration tests have been performed to calibrate the thermal model and the methodology that will be used latter to reconstruct the thermal properties of the multilayer assembly (i.e. Titanium panel combined with two Aeroguard blankets).

Four calibration tests have been executed by varying both the temperature setpoint of the furnace (i.e. 250 and 500°C) and the pressure setpoint in the cell (i.e. Patm and ~400Pa). The following figure shows the temperature evolution measured on the titanium panel (front face), on both sides of the Macor plate and on the internal partition (front face). The pressure in the cell stays constant during the entire test. The time $t=0$ corresponds to the insertion of the cell inside the furnace. We can see that the Macor plate reaches its thermal equilibrium (variation < 1% of final value) after 4500 sec and 2500 sec for the tests at respectively 250°C and 500°C. We can also see that the test pressure does not influence significantly this time. Since the Macor is a zero-porosity material, its thermal properties will not depend on the pressure. Therefore, testing at evacuated conditions instead of atmospheric pressure, will only reduce the convection and conduction heat transfer inside the cell (air) and decrease the overall heat transfer though the front face. This is obviously not the case since the temperature drop measured across the Macor plate increases between the test at atmospheric pressure and the corresponding one under vacuum. This observation indicates that the heat transfer problem cannot be assumed as 1D and that the heat transfer from the side panels cannot be neglected if we want to reconstruct properly the experiments.

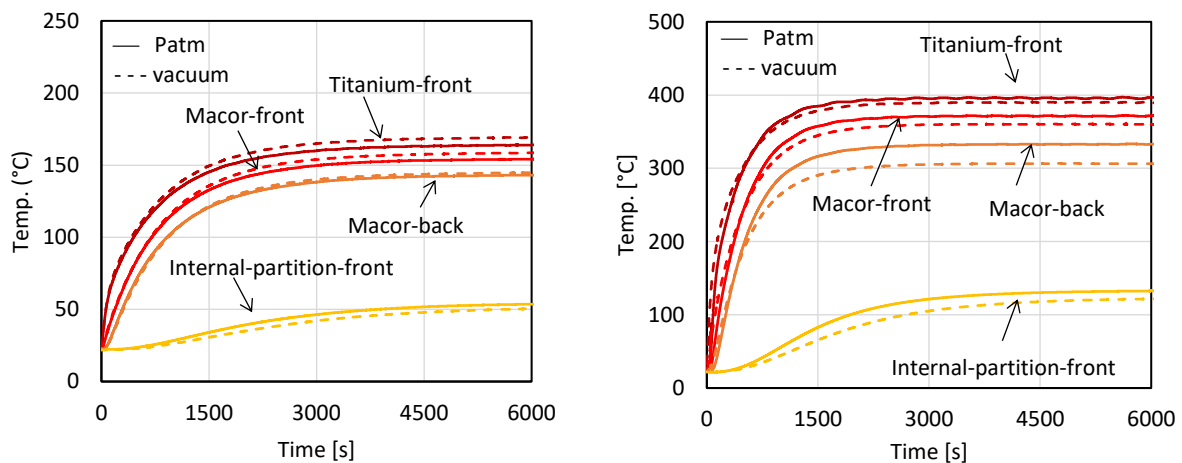


Fig. 4: Calibration tests with a furnace temperature set at 250°C (left) and 500°C (right)

2.3. Calibration of the nodal model

As highlighted in the previous paragraph, the heat transfer inside the test cell cannot be assumed as a one-dimensional problem and the thermal model should take into account the heat transfer through the side panels. Fig. 5-left presents the architecture and the discretization of the corresponding 3D model. The different panels of the cell are modelled with only one node located at the center of the panel. It is useless to add more nodes in the normal direction since the temperature will be uniform along this direction (low wall thickness and heat conductive material). On the contrary, adding more

nodes in the transversal direction (especially for the side panels) would be an interesting improvement in the future. The Macor plate is modelled in the normal direction with 10 nodes (1 node per mm). There is no discretization in the transversal direction. Finally, the internal air cavities and the external environment are modelled with one node.

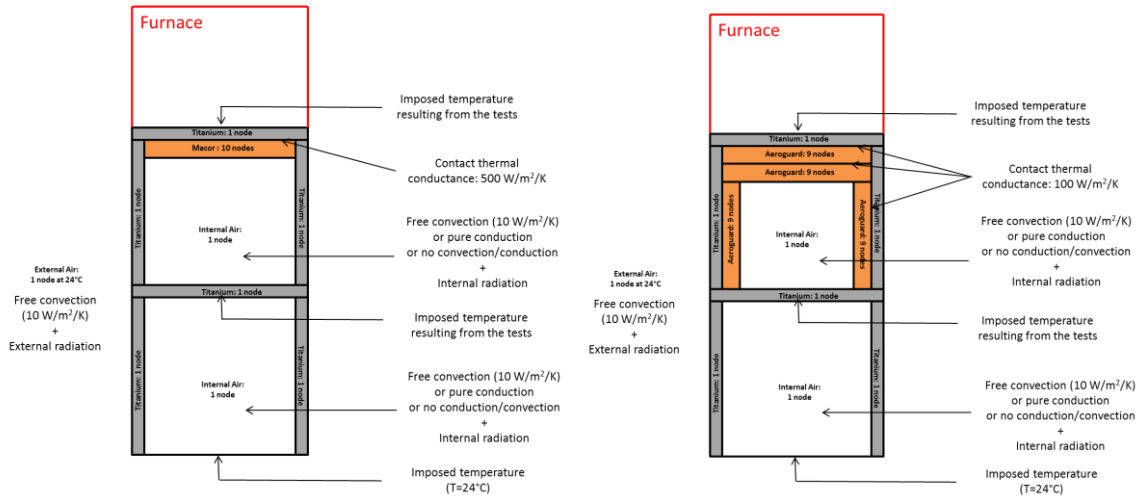


Fig. 5: Thermal model for the calibration tests (left) and for the second series of tests (right)

The Fig. 5 (left) shows also the boundary conditions used in the thermal model. It has been decided to impose directly as boundary conditions the measured temperature on the front face exposed to the furnace. Indeed, modelling the heat transfer between the furnace walls (in red) and this face would have introduced additional errors without adding any interesting insight to our problem. Also the temperature of the internal partition has been set to its measured value to not introduce unnecessary inaccuracy. All conductive heat transfer between the nodes are modelled. All thermal contacts are assumed as perfect expect for the one between the Macor plate and the Titanium panel for which the thermal conductance has been calibrated from the test results and applied to the model ($C=500W/m^2/K$). The temperature of the external environment has been fixed to 24°C. The external faces are exchanging with this environment both by natural convection (standard coefficient $h=10W/m^2/K$) and by radiation (surface emissivity $\epsilon = 0.9$). The internal faces are exchanging between each other by radiation (surface emissivity $\epsilon = 0.9$). Different types of conductive/convective heat transfer have been considered between the internal faces and the air inside the cell depending on the pressure level:

- Atmospheric pressure: (I) natural convection ($h=10W/m^2/K$) (II) pure conduction
- Vacuum pressure: (I) pure conduction (II) no conduction and no convection

The model uses temperature-dependent thermal properties for the different materials [8].

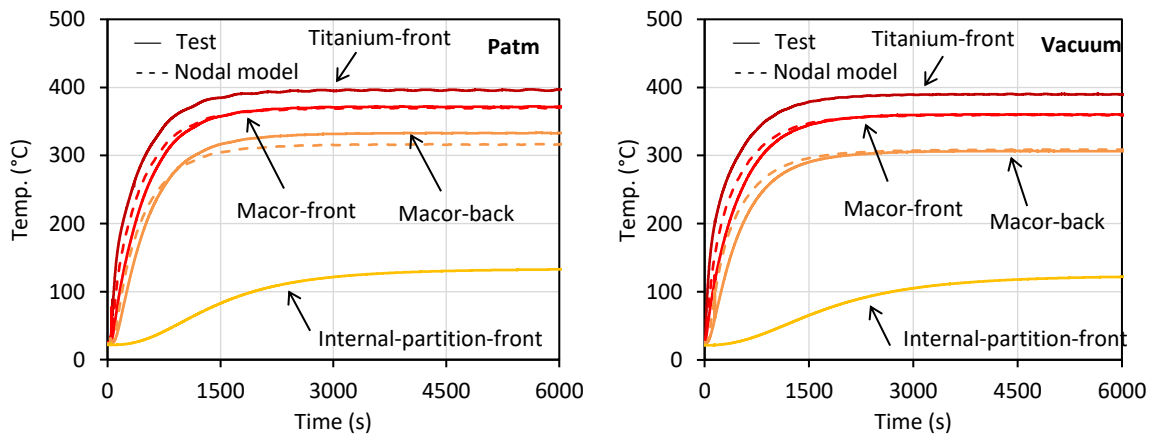


Fig. 6: Calibration of the nodal model at temperature setpoints of 500°C and two different pressure setpoints (Patm and vacuum) (pure conduction between internal faces on the cell and internal air)

The Fig. 6 compares the temperature predicted by the model on both sides of the Macor plate with the measured values for a furnace temperatures of 500°C) and two different pressures in the test cell (i.e. Patm and ~400Pa). Note that logically there is no difference between the measured and predicted values for the titanium face and the internal partition since the measured temperatures have been imposed as boundary conditions in the model. The numerical results shown in Fig. 6 have been obtained assuming pure conductive heat transfer between the internal faces of the cell and the air inside the cell.

In general, the temperature on both sides of the Macor plate are well predicted by the model especially when the cell is evacuated. The small deviation observed at atmospheric pressure might come from a larger contribution of the heat transfer through the side faces. Indeed, the model could not reproduce accurately this heat transfer due to the poor discretization of the side panels and air cavities. For the same reason, it is difficult to draw conclusions on the most appropriate type of heat transfer between these panels and the air inside the cell (pure convection / pure conduction / no conduction and no convection).

2.4. Thermal test

A first campaign of tests was conducted in the configuration of the Fig. 5-left with the macor replaced by 2 layers of Aerogard material. The first interesting information to extract from this first series of tests concerns the effect of the pressure on the thermal equilibrium. The Fig. 7 plots the temperature drop across the Aerogard blankets versus the pressure. As expected, this quantity increases when the pressure goes from atmospheric to vacuum pressure, indicating that the overall thermal conductivity of the assembly is lower at low pressure. For the test 1, the blanket was not properly in contact with the titanium box. This point must be excluded.

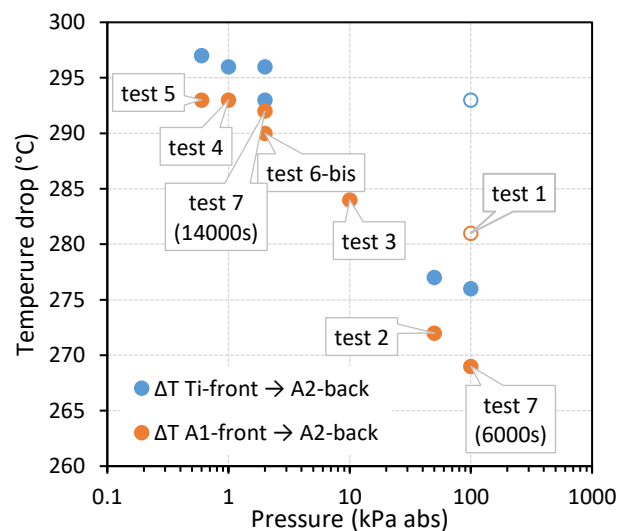


Fig. 7: Effect of the pressure on the thermal equilibrium (temperature drop across the assembly)

The analysis of the model predictions and their comparison with the corresponding test data has shown that the back of the test assembly receives a non-negligible heat flux from the side panels of the box. Since the model is not capable to reproduce accurately this heat flux, it has been decided to limit it as much as possible in the experimental set-up by adding an extra-insulation.

A second series of tests has been conducted with a modified configuration of the cell in order to limit the back heating of the test assembly. The side panels has been insulated as illustrated in the Fig. 5-right. The existing thermal model of the cell has been adapting to the new configuration. Fig. 5 (right) shows the architecture of the modified model with its discretization scheme and its boundary conditions. This nodal model is similar to the one used to simulate the first series of tests except for the insulation

layer added at the back of the side panels. The same value of contact conductance ($C=100\text{W/m}^2/\text{K}$) than for the first series of tests has been added between the Titanium panel and the first blanket as well as between the first and the second blanket.

The first simulations reproduce the test at atmospheric pressure (constant pressure). Fig. 8 (left) compares the temperature predicted by the model with the measured ones. The temperature on the front Titanium panel and on the internal partition have been imposed as boundary conditions in the simulations. As for the first series, two different heat-transfer mechanisms have been considered between the internal faces of the cell and the air inside the cell: a natural convection mechanism with a coefficient $h=10\text{W/m}^2/\text{K}$ and a pure conduction mechanism. The numerical results shown in Fig. 8 have been obtained by activating a natural convection heat transfer. We can see on this figure that the temperature evolution is relatively well reproduced by the model indicating that the thermal properties of the Aeroguard blanket at atmospheric pressure are correct. The simulation done by activating a pure conduction heat transfer inside the cell (instead of a natural convection heat transfer) is not correctly reproducing the test. This result seems logical since the cell is not evacuated for this test.

The second simulations reproduce the test at the lowest pressure ($P=600\text{Pa}$). Fig. 8 (right) compares the temperature predicted by the model with the measured ones. Two different heat-transfer conditions have been considered between the internal faces of the cell and the remaining air inside the cell: a pure conduction heat transfer and no heat transfer (no convection / no conduction). The numerical results have been obtained with the condition "no heat transfer". No significant difference has been observed with the predictions done by considering a pure conduction heat transfer between internal face and internal air. As for the first series, a factor of 0.3 has been applied to the thermal conductivity of the Aeroguard at atmospheric pressure to transpose it to vacuum conditions. We can see that this correction allows reproducing perfectly the temperature evolution measured at the different interfaces of the test assembly.

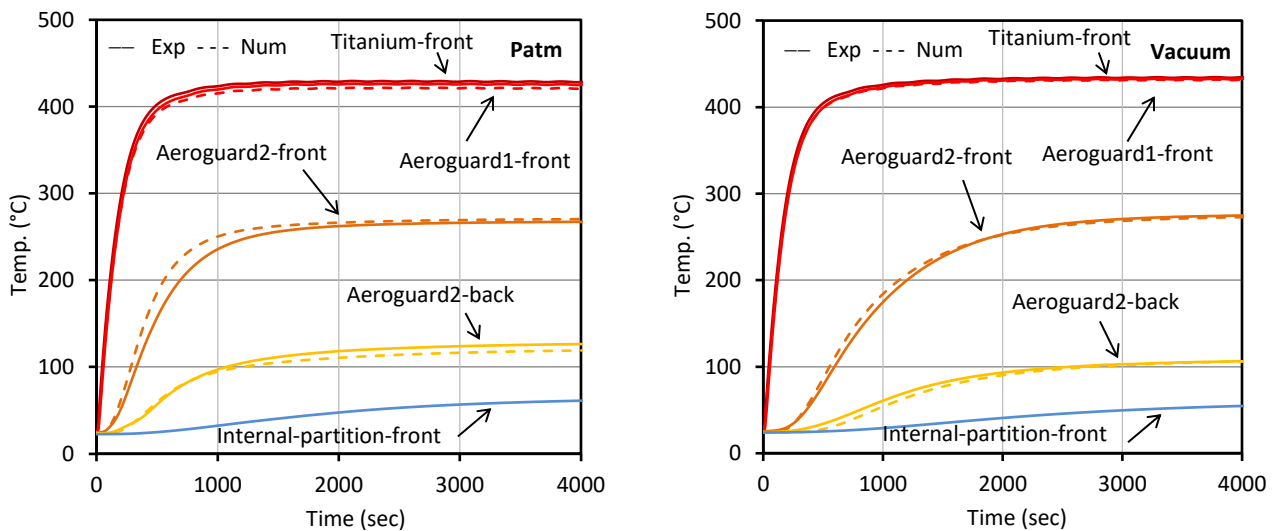


Fig. 8 : Numerical simulations (nodal model) of the second series of tests (left: test 8 at Patm; right: test 9 at 600Pa)

2.5. conclusions and recommendations

The heat transfer through a representative multilayer assembly, i.e. titanium shell combined with two Aeroguard blankets on its backside, has been characterised experimentally at representative pressure evolution experienced during the flight, i.e. from ambient pressure down to near vacuum. A 3D thermal nodal model has been built to reproduce these experiments and to calibrate the thermal properties of the multilayer assembly. The methodology has been first validated by replacing the two Aeroguard blankets by a zero-porosity material with well-known thermal properties (Macor). After this validation, a first series of tests has been conducted and compared to the numerical predictions of the nodal model. This first analysis has identified that the thermal conductivity k of the Aeroguard blanket

provided by PROMAT was good at atmospheric pressure but not correct at vacuum pressure. A correction factor calibrated from the test data has been proposed ($k_{vacuum} = 0.3 k_{atm}$). This analysis has also pointed out that the test data are biased by a back heating of the multilayer assembly. It was clearly identified thanks to high-fidelity conjugated heat transfer simulations that this back heating was coming from the sidewalls of the test cell. Since the nodal model was not capable to reproduce this lateral heat transfer (insufficient number of nodes in the considered direction), it has been decided to modify the experimental set-up by insulating the sidewalls of the cell such that to prevent any back heating of the test assembly. A second series of tests have been conducted on this new configuration. The nodal model was capable to reproduce faithfully the test results confirming that the properties of the Aeroguard blankets.

Several recommendations could be envisaged for future tests:

- The thermal tests have been conducted with the standard-duty product (SD). The outer envelope of this standard product is made with a textile covering material rated at only 500°C. The test temperature has been adapted accordingly. However, the flight blankets should be made from a heavy-duty product (HD) covered with a textile rated at 1000°C in order to be compliant with the specifications [9] (i.e. maximum temperature of 700°C). The tests could therefore be repeated at higher temperature with this heavy-duty product to validate their thermal properties up to 700°C.
- The nodal model shows some limitations to reproduce the heat transfer along the lateral direction. Increasing the number of nodes along this direction would definitely help to better capture this lateral heat transfer.
- The experimental set-up could also be improved to better compare the results with the model predictions. For instance, it would be valuable to insert more thermocouples on the titanium panels of the cell and to use the measured temperature as boundary conditions of the model. Also, the results from the second series of tests has shown that there is probably still a small back heating even with the insulated test cell. We would recommend to reinforce this insulation by adding a second blanket on back of the side panels.

3. Qualification of the external TPS of the ESM exposed to hypersonic flow

The objective of this part is to characterise experimentally these blankets on a ground facility with representative external flow exposure. The design of the test articles and of the sample holder has been detailed in the technical note D4010 [10]. A first campaign was carry out with the Aeroguard 160SD [11]. In this campaign four material are investigated: Aeroguard 160SD, 190SD, 160HD and 190HD.

3.1. Hypersonic wind tunnel

The tests was executed in the VKI's hypersonic wind tunnel H-3 (Fig. 9). This tunnel is a blow-down facility with an axisymmetric nozzle giving a uniform Mach 6 free jet 12 cm in diameter. Air is supplied from a pebble-bed heater at stagnation pressures from 7 to 35 bar and a maximum stagnation temperature of 550K. Reynolds number may be varied from 3×10^6 to 30×10^6 /m. The test section contains a three-degree of freedom traversing system for model and/or probe support that allows the angle of incidence to vary between -5 to +5 degrees. A mechanism for rapid injection of model is available. Instrumentation includes shadow and schlieren systems, pressure scanner for pressure measurements, a three-component strain gauge balance, equipment for heat transfer measurements including infrared camera and oil-fil interferometry for skin-friction measurement.

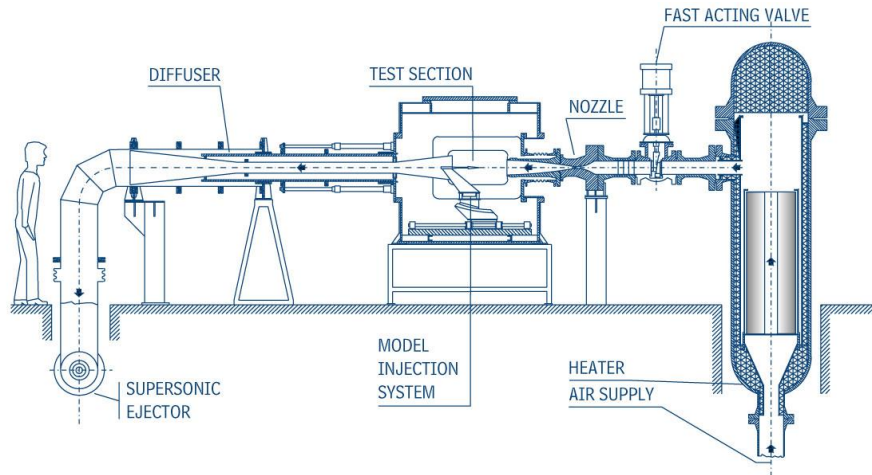


Fig. 9: Mach 6 hypersonic wind tunnel H-3

3.2. Test similitude

The case study for the experimental characterisation of the blankets to external hot flow is the openings on the Experimental Support Module (ESM) at the connection points with the struts toward the Experimental Flight Test Vehicle (EFTV). Fig. 10 shows one of those opening. The corresponding surface area and perimeter are respectively 0.042m^2 and 0.84m .

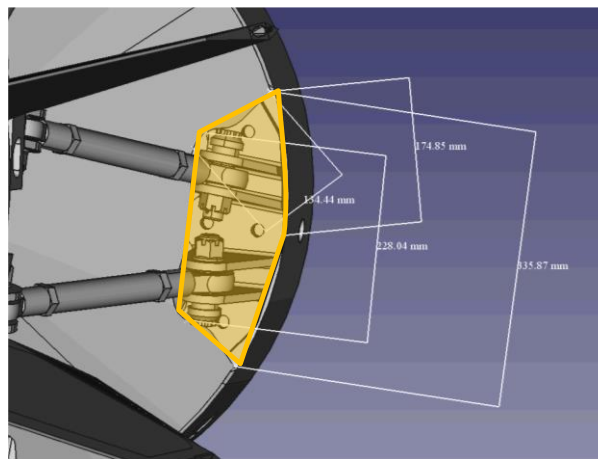


Fig. 10: ESM openings at the connection points with the struts towards EFTV

The flight conditions considered for the case study in agreement with the ESA-TO are the following ones:

- Angle of Attack: 60°
- Dynamic pressure: 3.2kPa
- Static pressure: 76Pa

The test methodology consists of duplicating the flight configuration to the ground test configuration the ratio between the pressure forces seen by the exposed blankets and their perimeter. Indeed, the blankets placed at the ESM openings shall be attached to the vehicle structure only at their periphery.

Applying the Newtonian flow theory to the flight configuration gives a pressure of 5600 Pa on the blankets exposed to the external hot flow. In the wind tunnel, the model is exposed to a Mach 6 free-jet with a stagnation temperature T_0 of 500K and a stagnation pressure p_0 from 10×10^5 to $30 \times 10^5\text{ Pa}$. The following table gives the corresponding range of dynamic pressure p_{dyn} that can be achieved in this test facility.

Mach	p_0 [Pa]	p [Pa]	T_0 [K]	ρ_∞ [kg/m ³]	u_∞ [m/s]	p_{dyn} [Pa]
6.00	1000000	633	500	0.0362	939	15960
6.00	2000000	1267	500	0.0724	939	31919
6.00	3000000	1900	500	0.1086	939	47881

Table 1: H-3 test conditions

The Newtonian flow theory is applied again to these test conditions to retrieve the flow pressure seen by the test sample at different Angles of Attack (AoA) and different stagnation pressures (Fig. 11). Note that the AoA should be kept as low as possible to avoid a blockage of the tunnel.

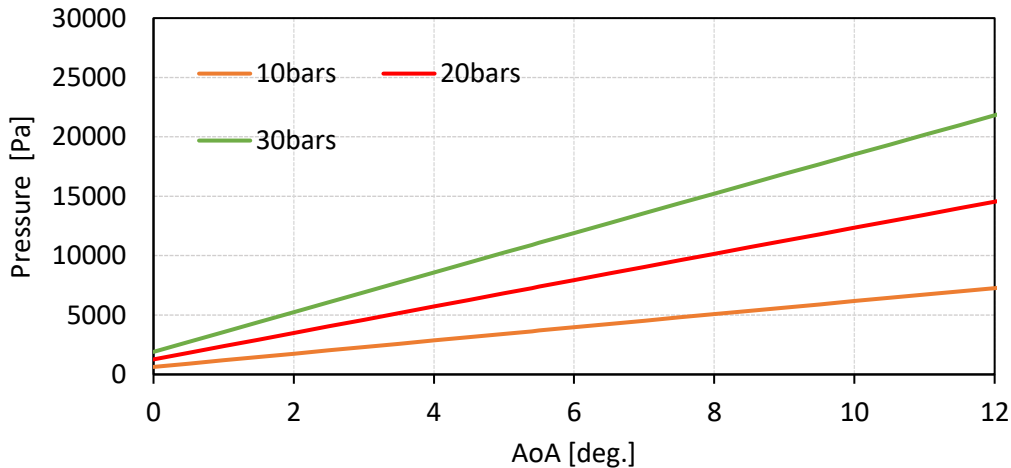


Fig. 11: Pressure duplication between flight and test configurations.

The following figure plot the corresponding ratio - pressure force / perimeter - assuming a perimeter of 0.4m for the test sample (rectangular sample 120x80mm). Based on this graph, a good matching condition with the flight could be reached with an AoA of 6 degree and a stagnation pressure in the wind tunnel of 30X10⁵ Pa. it was decided to reduce the total pressure and to perform the test up to AoA of 7.5 degree.

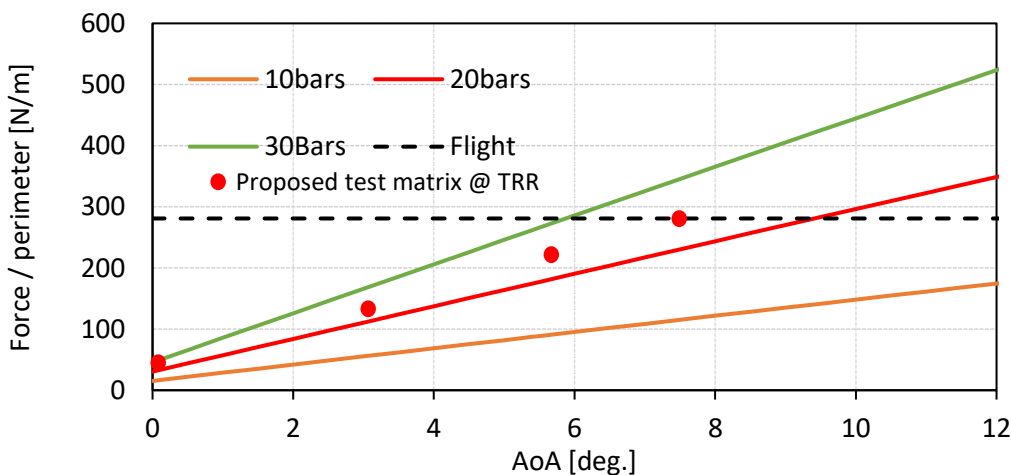


Fig. 12 : Duplication of the ratio "pressure force / perimeter" between flight and test configurations

3.3. Tests results

In the first campaign, the three tests at AoA=3°, 5.4° and 7.5° were successful. The last one was performed at conditions duplicating the flight configuration, i.e. same ratio pressure forces over

perimeter. The high-speed images do not show any visible degradation nor excessive bending of the blanket during its exposure to the flow.

The first test was at zero incidence. This test failed only 1650ms after injecting the sample into the flow. The excessive deformation of the blanket visible in the video leads to its ripping and the core material of the blanket (white silica powder) is released in the flow. This brutal rupture of the blanket creates a fast upward displacement of the leading edge of the model. This leads to a permanent deformation of the sample holder at its weakest point just upstream the second wedge at the trailing edge.

A second campaign was performed. Four different grades of Aeroguard blankets are considered for these complementary tests: 160-SD, 160-HD, 190-SD and 190-HD. This combination allows testing two different core material densities, i.e. 160kg/m^3 and 190kg/m^3 and two different covering textiles, i.e. Standard Duty textile rated at 500°C and Heavy Duty textile rated at 1000°C . The mechanical resistance of the plate was studied by FEM, especially at 0° . A new reinforced model was designed and manufactured to avoid possible deformation at 0° .

The test matrix is composed of 8 tests: the 4 grades of the Aerogard blankets are tested at 7.5° and 0° .

The four tests at $\text{AoA}=7.5^\circ$ were successful. They were performed at conditions duplicating the flight configuration, i.e. same ratio pressure forces over perimeter. The high-speed images do not show any visible degradation nor excessive bending of the blanket during its exposure to the flow.

Three tests were performed at zero degree of incidence. For all of them, the sample was damaged after only one or two seconds of exposure to the flow. The destruction is always at the same location, close to the end of the plate. Only the front part of the sample still contains powder. At that point, it was decided to adapt the test matrix to better understand the phenomena involved in the damage of the samples.

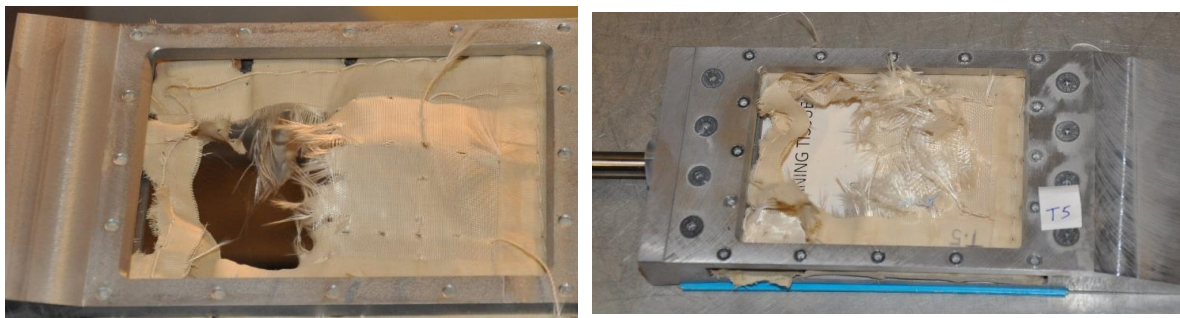


Fig. 13: Sample after a test @ 0°

We analysed in detail the high-speed videos to understand the phenomena involved in the destruction of the samples. It appeared that the problem was initiated at the end of the plate. Air enters inside the material, which blows up under the pressure. The pressure in this configuration should not be high enough to damage the material.

It was decided to replace the blanket sample by a rigid plate in aluminium in order to record schlieren images and collect information about the flow at 0° incidence. A blockage of the wind tunnel was observed after 1.5 second. It was not the destruction of the material that produced blockage but the blockage that destroyed the material (see Fig. 14-left). The picture shows clearly the limit of the over-expanded jet crossing the shock coming from the leading edge. The second shock is induced by the separation of the boundary layer.

In order to avoid this blockage, an easy solution consists in turning the plate upside down. The Fig. 15 gives the shock topology for the two mounting configurations. The diffuser is open at the bottom to allow the passage of the model and its support. As seen on this figure, in the nominal configuration, the bottom shock is not captured by the diffuser. By turning the plate upside down, the shock angle is smaller at the bottom and can be captured. The schlieren picture obtained in this configuration is shown in the Fig. 14-right.

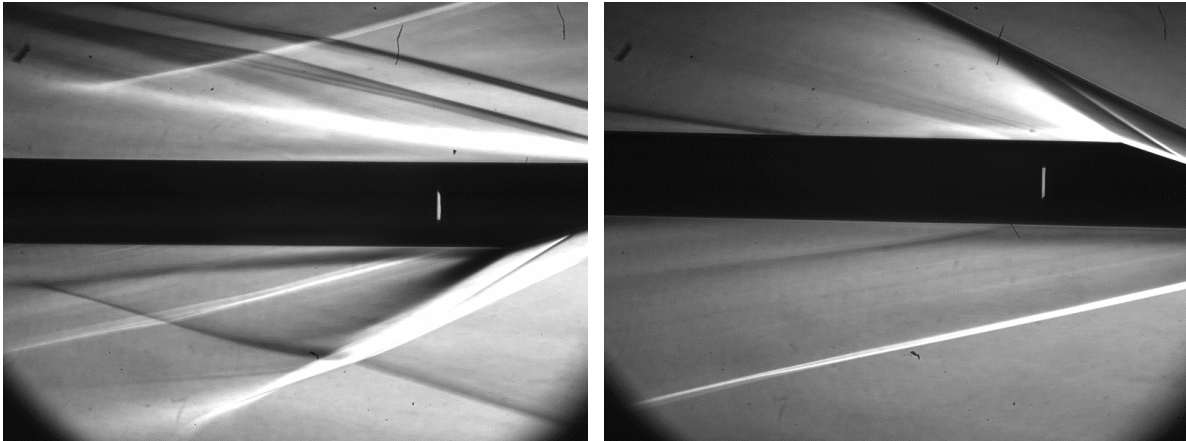


Fig. 14: Schlieren picture – Test #10 @ 1s (left) – Test #11(right)

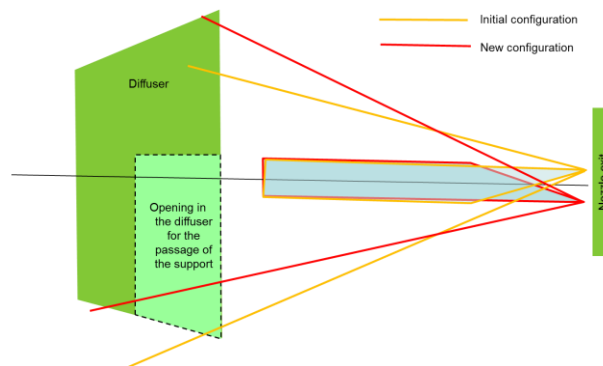


Fig. 15: Schema of the shock topology

As extra samples were supplied for the four grades of Aeroguard, the tests at zero degree incidence have been repeated with new samples. These repetitions were successful. There is no visible degradation of the blankets.

3.4. conclusions

An experimental characterisation of the blanket exposed to external flow has been proposed. The Newtonian flow theory has been applied to duplicate the configuration from flight to ground. In this second campaign, four different grades of Aeroguard have been tested (160SD, 190SD, 160HD, 190HD). The tests at 7.5° were successful and no damage was observed on the sample whatever the grade. The test at zero incidence surprisingly failed and further investigation was carry out to understand the problem and solve it. The tests at zero degree were finally repeated successfully for all the grades.

4. Mechanical tests and characterization of the fixations

The purpose of these static load tests performed at the Large Diameter Centrifuge (LCD) at ESA/ESTEC is to qualify the fixations of the AEROGUARD insulation panels on the structure of the vehicle. These insulation panels will be subjected to high acceleration loads during the ascent of the vehicle and during the pull-out manoeuvre of the vehicle. As the range of acceleration does not exceed 11g according to specifications [9], it was decided to perform at minimum all the tests at this load in any direction. The test matrix has been slightly adapted during the test campaign based on the observations made in order to optimise the test time (1-day) available at the Large Diameter Centrifuge.

4.1. Gondolas

The LDC consists of the following subsystems shown in Fig. 16

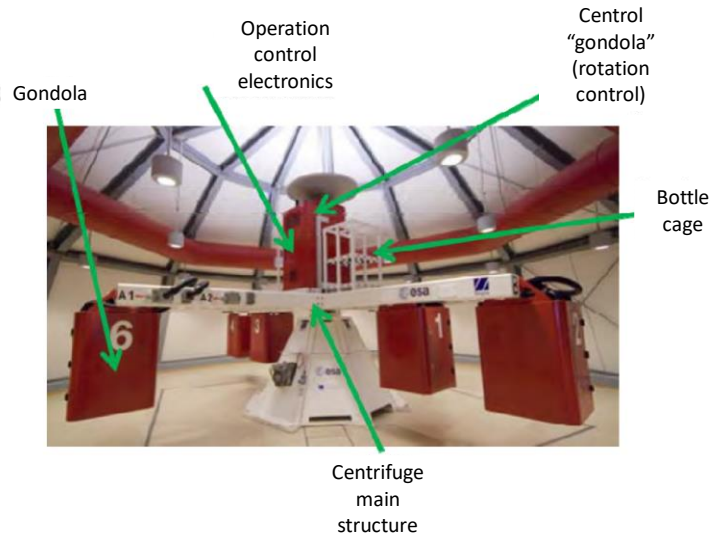


Fig. 16: LDC main structures

The centrifuge main structure is the center of the system. It is equipped with four rotor arms, a central gondola for the control of experiments. The gondola is attached to the rotor and is equipped with swing shaft for arms positioning. It contains scientific data interfaces (serial, USB, Ethernet, analogue video), power and sensors (temperature and accelerometers). A dedicated structure is anchored to the gondola housing in order to position the AEROGUARD insulation panels along different acceleration axis. This structure is composed of Aluminium profiles (Bosch Rexroth) on which are attached three Aluminium plates (6mm thick) as shown in Fig. 17. The plate or frame A-A is fixed to the left side of the gondola housing. Note that this frame will be exposed to a transversal acceleration (oriented downward) during the test. The second frame B-B is fixed to the top side of the gondola housing. This frame will be exposed to a normal acceleration. Finally, the last frame C-C is fixed to the backside of the gondola facing a transversal acceleration during the test (oriented downward).

4.2. AEROGUARD flexible insulation panels

AEROGUARD is a highly flexible microporous insulation panel designed for aerospace and aeronautical applications. It is available in four different densities and various textile covering the insulant materials. The version provided by PROMAT for the static load tests is AEROGUARD-160 ($\rho=160\text{kg/m}^3$) with E-glass textile (SD Standard Duty). Since this textile is rated only up to 500°C , it will be replaced in the vehicle by silica cloth (HD High Duty) rated up to 1000°C . The panels have been tailored made from large panels in order to fit on the supporting frames. The acceleration will be applied to an assembly of two panels attached to the back frame (aluminium plate). The thickness of each insulation panels is 9mm. Different types of fastening solutions are added to the panels (stitched to the textile): 4 straps made with Velcro, 4 straps made with textile, 4 Velcro patches on each side or a traversing sheath made in textile to pass a metallic cable. Finally, sheaths made in textile and stitched in the center of panels have been added to panels #2 and #3 in order to incorporate a mass simulating an electrical connector and/or other items being fixed or connected to the Aeroguard panels (illustration in the Table 2).

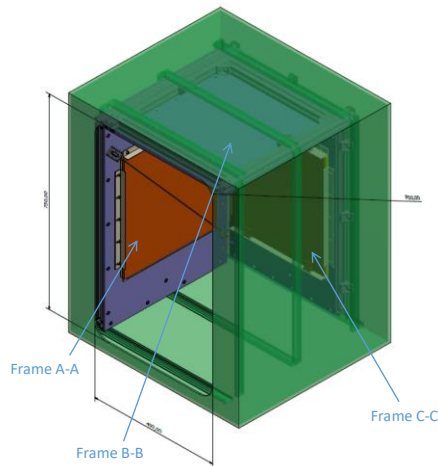


Fig. 17: Views of the gondola equipped with the supporting frames

4.3. Test

The static load tests have been performed at the Large Diameter Centrifuge (ESA/ESTEC) on February 20th 2019. A technical support has been provided by the LIS lab personnel to operate the facility as well as for the installation of the supporting frames inside the gondola.

The table below reports the real test conditions applied for each test as well as the observations made after test. The second column of this table indicate which frames the panels are installed (A-A, B-B or C-C) and the direction of the acceleration. In the final runs 6 to 8, a maximum load of 16g was applied as well. For certain cases, an incremental rise in g-load was applied to increase the resolution level at which the panel or related fastening might fail.





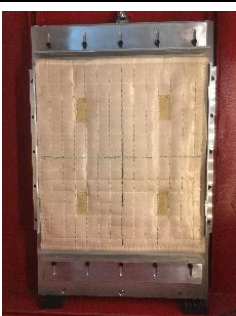
4.4. Conclusion






The following conclusions can be drawn after these static load tests performed at the Large Diameter Centrifuge:



- The Velcro patches bonded on the aluminium plate (back) with the ASIFLEX glue debond at high load. The glue remains on the Aluminium plate but not on the Velcro path.
- The fastening solution with a traversing cable resists to the static load applied but it is suspected that in case of combined load (axial + normal), any unsupported corners of the AEROGUARD panels will bend (twist) around the cable. This would demand for a cross wire as a final solution.
- The straps in Velcro are very efficient. This solution was tested in the requested range of acceleration (11g) and even higher (16g). It was also tested while doubling the applied mass in the straps representing the electrical connectors.

It is recommended to take care of the structure finishing on which the straps are fixed. It must be manufactured with round corners to avoid cutting the straps.

Table 2: Test results

Run	Frame	Panels (before)		Fixation wall - front panel	Fixation front - back panels	Fixation back panel - frame	g	Observations
1	AA (J)		Font panel: #4 Back panel: #7	No	No	Cable with protective sheath tube	11g ~5min	No issue. All panels still in place and in good shape after 5 min
1	CC (I)		Front panel: #5 Back panel: #2	No	No	4 straps with Velcro (top/bottom)	11g ~5min	No issue. All panels still in place and in good shape after 5 min
1	BB (⊗)		Front panel: #1 Back panel: #6	No	No	4 straps with Velcro (left/right)	11g ~5min	No issue. All panels still in place and in good shape after 5 min
2	AA (J)		Front panel: #4 Back panel: #8	4 Velcro patches	4 Velcro patches	Cable with protective sheath tube	11g ~5min	Panels in place after test. 1 Velcro patch on aluminium plate unglued (re-glued after test). Except that no issue.
2	CC (I)		Front panel: #5 Back panel: #6	4 Velcro patches	4 Velcro patches	No	11g ~5min	No issue. All panels still in place and in good shape after 5 min.

Run	Frame	Panels (before)		Fixation wall - front panel	Fixation front - back panels	Fixation back panel - frame	g	Observations
5	CC (↓)		Front panel: #5 Back panel: #1	No	No	4 straps with Velcro (left/right)	11g ~5min	No issue. All panels still in place and in good shape after 5 min.
5	BB (⊗)		Front panel: #6 Back panel: #4	4 Velcro patches	4 Velcro patches	No	11g ~5min	Back panel detached during acceleration ramp-up. Front panel detached after 4 min at 11g.
4	CC (↓)		Front panel: #4 Back panel: #8 + mass 166g	4 Velcro patches	4 Velcro patches	No	4g ~1min 8g ~1min 11g ~5min	No issues. Panels still in place after test.
6	BB (⊗)		Front panel: #2 + mass 228g	No	No	4 straps with Velcro (top/bottom)	1g ~1min 4g ~1min 8g ~1min 11g ~5min 12g ~2min stop 16g ~5min	Panels bend but stay in place. Go back +/- to position after test. No issues.
7	AA (↓)		Front panel: #5 Back panel: #8 + mass 166g	No	No	Cable	4g ~1min 8g ~1min 11g ~5min 16g ~5min	No issues. Panels still in place after test.

Run	Frame	Panels (before)		Fixation wall - front panel	Fixation front - back panels	Fixation back panel - frame	g	Observations
7	CC (1)		Front panel: #6 Back panel: #2 + mass 228g	No	No	4 straps with Velcro (top/bottom)	4g ~1min 8g ~1min 11g ~5min 16g ~5min	No issues. Panels still in place after test.
8	BB (⊗)		Front panel: #5 Back panel: #3 + mass 114g	No	No	3 Straps (top /bottom) (1 strap damaged prior test and replaced by cable ties)	11g ~5min 16g ~5min	Rupture of the tissue of 1 strap during start-up (cause: slots w/ sharp edges, tissue damaged during assembly). Test stopped and strap replaced with cable ties. Test restarted. 2 remaining straps passed the test. Visible damage on their tissue but no rupture. Recommendation: careful assembly, remove sharp edges

References

1. Steelant J., 'Achievements Obtained for Sustained Hypersonic Flight within the LAPCAT Project', 15th AIAA International Space Planes and Hypersonic Systems and Technologies Conference, AIAA-2008-2578, 28 April- 01 May 2008, Dayton, Ohio, USA.
2. Steelant, J., Varvill R., Defoort S., Hannemann K. and Marini M., 'Achievements Obtained for Sustained Hypersonic Flight within the LAPCAT-II Projet', 20th AIAA International Space Planes and Hypersonic Systems and Technologies Conference, AIAA-2015-3677, 5-8 July 2015, Glasgow, Scotland.
3. Steelant J., 'ATLLAS: Aero-Thermal Loaded Material Investigations for High-Speed Vehicles', 15th AIAA International Space Planes and Hypersonic Systems and Technologies Conference, AIAA-2008-2582, 28 April-01 May 2008, Dayton, Ohio, USA.
4. Steelant J., Dalenbring M. ., Kuhn M., Bouchez M. and von Wolfersdorf J., 'Achievements obtained within the ATLLAS-II Project on Aero-Thermal Loaded Material Investigations for High-Speed Vehicles', 21st Int. Space Planes and Hypersonic Systems and Technology Conference, AIAA-2017-2393, 6-9 March 2017, Xiamen, China.
5. Steelant J., Langener T., Hannemann K., Riehmer J., Kuhn M., Dittert C., Jung W., Marini M., Pezzella G., Cicala M. and Serre L., 'Conceptual Design of the High-Speed Propelled Experimental Flight Test Vehicle HEXAFLY', 20th AIAA International Space Planes and Hypersonic Systems and Technologies Conference, AIAA-2015-3539, 5-8 July 2015, Glasgow, Scotland
6. Andro J.Y, Scigliano R., Kallenbach A., Steelant J., Thermal Management of the Hexafly-Int Hypersonc Glider, 1st International Conference on High Speed Vehicle Science Technology, 26-29 November 2018, Moscow, Russia
7. J-B Gouriet, J. Freitas Monteiro and S. Paris, "Design of the thermal cell with variable pressure", GSTP Lightweight flexible microporous insulation panel, ESA contract n°4000125358/18/NL/KML/zk, deliverable D3010, Oct-2019
8. Boivineau et al., "Thermo-physical Properties of Solid and Liquid Ti-6Al-4V (TA6V) Alloy", Int. J. of Thermophysics, Vol 27, March 2006, except for ϵ)
9. J-Y Andro and J. Steelant, "Requirements and Load Case Definition for the TCS protection of the ESM and EFTV", HEXAFLY-INT deliverable D6.2.9 - Promat, Rev. 7.
10. J-B Gouriet and S. Paris, "Design of the sample holder for external flow exposure", GSTP Lightweight Flexible Microporous Insulation Panel, ESA Contract No. 4000125358/18/NL/KML/zk, Deliverable D4010
11. B Gouriet and S. Paris, "Experimental characterisation of flexible microporous blankets exposed to external hot flow", ESA Contract No. 4000125358/18/NL/KML/zk, Deliverable D4020